Materials Today Bio 27 (2024) 101114

Contents lists available at ScienceDirect

Materials Today Bio

journal homepage: www.journals.elsevier.com/materials-today-bio

High-precision bioactive scaffold with dECM and extracellular vesicles targeting 4E-BP inhibition for cartilage injury repair

Yu Han [a,d,1], Yixin Dong [a,1], Bo Jia [b], Xiangyu Shi [a], Hongbo Zhao [a], Shushan Li [a], Haitao Wang [a,***], Binbin Sun [c,**], Li Yin [a,*], Kerong Dai [d]

[a] Department of Orthopaedics, Medical 3D Printing Center, The First Affiliated Hospital of Zhengzhou University, Zhengzhou, 450052, China
[b] Department of Orthopedics, Shanghai General Hospital, Shanghai Jiao Tong University School of Medicine, Shanghai, 200080, China
[c] Shanghai Engineering Research Center of Nano-Biomaterials and Regenerative Medicine, College of Biological Science and Medical Engineering, Donghua University, Shanghai, 201620, China
[d] Department of Orthopedic Surgery, Shanghai Key Laboratory of Orthopedic Implants,Clinical and Translational Research Center for 3D Printing Technology, Shanghai Ninth People's Hospital, Shanghai Jiao Tong University School of Medicine, Shanghai, 200011, China

ARTICLE INFO

Keywords:
dECM
Extracellular vesicles (EVs)
Eletro-writing
4ebp
Cartilage repair

ABSTRACT

The restoration of cartilage injuries remains a formidable challenge in orthopedics, chiefly attributed to the absence of vascularization and innervation in cartilage. Decellularized extracellular matrix (dECM) derived from cartilage, following antigenic removal through decellularization processes, has exhibited remarkable biocompatibility and bioactivity, rendering it a viable candidate for cartilage repair. Additionally, extracellular vesicles (EVs) generated from cartilage have demonstrated a synergistic effect when combined with dECM, potentially mitigating the inhibitory impact on protein synthesis by phosphorylating 4ebp, thereby promoting the synthesis of cartilage-related proteins such as collagen. In pursuit of this objective, we have innovated a novel bioink and repair scaffold characterized by exceptional biocompatibility, bioactivity, and biodegradability, establishing a tissue-specific microenvironment conducive to chondrogenesis. Within rat osteochondral defects, the biologically active scaffold successfully prompted the formation of transparent cartilage, featuring adequate mechanical strength, favorable elasticity, and dECM deposition indicative of cartilage. In summary, this study has effectively engineered a hydrogel bioink tailored for cartilage repair and devised a bioactive cartilage repair scaffold proficient in instigating cell differentiation and fostering cartilage repair.

1. Introduction

Articular cartilage plays a pivotal role in joint functionality by offering essential functions such as lubrication, cushioning, and shock absorption [1]. Regrettably, both traumatic incidents and prolonged usage can induce the degeneration of cartilage, ultimately culminating in the onset of arthritis [2]. This, in turn, has prompted a substantial increase in healthcare expenditures dedicated to arthritis treatment on a global scale, marking a significant focus within the medical field [3]. Addressing cartilage damage emerges as a formidable obstacle in orthopedic research, primarily due to the inherent incapacity of cartilage to undergo self-repair, attributed to its absence of blood vessels and nerves [4].

The extracellular matrix (ECM) constitutes a pivotal element in the cellular microenvironment. Decellularized extracellular matrix (dECM) emerges through the process of removing cellular constituents from the

Abbreviations: Agc, aggrecan; BC, Blank Control; BMSCs, bone marrow mesenchymal stem cells; CCK-8, Cell Counting Kit-8; Col II, collagen II; DAPI, 4′,6-diamidino-2-phenylindole; dECM, Decellularized extracellular matrix; ECM, extracellular matrix; eIF4E, eukaryotic initiation factor 4E; eIF4G, eukaryotic initiation factor 4G; EVs, Extracellular Vesicles; EW, electro-writing; HE, Hematoxylin and Eosin; Lub, Lubrican; MSCs, mesenchymal stem cells; NTA, Nanoparticle Tracking Analysis; PE, PEGDA + dECM group; PEE, PEGDA + dECM + EVs group; PEGDA, polyethylene glycol diacrylate; rt-PCR, real-time polymerase chain reaction; TEM, Transmission Electron Microscopy; TGF-β, Transforming Growth Factor-β; WB, Western blotting; 4ebp, eukaryotic translation initiation factor 4E-binding protein.

* Corresponding author.
** Corresponding author.
*** Corresponding author.
E-mail addresses: wht870103@126.com (H. Wang), binbin.sun@dhu.edu.cn (B. Sun), liyin1966zzu@hotmail.com (L. Yin).
[1] These authors contributed equally to this work.

https://doi.org/10.1016/j.mtbio.2024.101114
Received 29 January 2024; Received in revised form 13 May 2024; Accepted 6 June 2024
Available online 8 June 2024

ECM, thereby effectively preserving its innate biological activity [5]. This decellularization method eliminates components that might incite immune responses while conserving active elements like collagen fibers, growth factors, and proteins that can stimulate stem cell differentiation and expression [6]. Moreover, constituents within the decellularized matrix can augment material biocompatibility, fostering enhanced adhesion and proliferation of stem cells. Employing decellularized matrix derived from the meniscus holds promise in furnishing tissue-specific growth factors and a conducive regenerative microenvironment for seeded cells, ultimately fostering amplified cell proliferation, differentiation, and the preservation of cellular phenotype [7].

Throughout the reparative process, Bone Marrow-Derived Mesenchymal Stem Cells (BMSCs) can be mobilized to the injury site, where they play a crucial role in secreting and orchestrating the local cellular environment. BMSCs, through paracrine pathways, engage in interactions with other cells, thereby exerting therapeutic effects [8,9]. Recent investigations underscore the significance of Extracellular Vesicles (EVs) in the context of cartilage repair. These nano-sized vesicles, with diameters ranging from 40 to 160 nm, encapsulate an array of bioactive substances, including proteins, nucleic acids, and lipids, capable of profoundly modulating the physiological functions of recipient cells. Beyond their role in recruiting Mesenchymal Stem Cells (MSCs) to the injury site, BMSCs also release EVs that serve to regulate the cellular microenvironment and facilitate interactions with other cells [10,11]. Emerging evidence posits that EVs create a microenvironment conducive to tissue regeneration, inhibiting chondrocyte apoptosis, promoting chondrocyte proliferation, and augmenting extracellular matrix synthesis [12,13]. Notably, studies such as that conducted by Tao et al. demonstrate the therapeutic potential of EVs overexpressing miR-140-5p, which can downregulate RalA expression and upregulate key chondrogenic genes (SOX9, ACAN, and Col II), exhibiting therapeutic efficacy in a rat model of osteoarthritis [14]. Furthermore, the integrin proteins present on the surface of EVs, along with other receptors, interact with the ECM, thereby promoting the differentiation of BMSCs [15]. Narayanan et al. have substantiated this phenomenon by showing that EVs significantly upregulate the expression of Runx2 and Osterix, thereby promoting the osteogenic differentiation of MSCs through binding to type I collagen hydrogel [16,17].

The intricate process of cartilage regeneration following injury in the human body is under the intricate regulation of various cells and signaling molecules. A pivotal player in this orchestration is the Transforming Growth Factor-β (TGF-β)/Smad pathway, assuming a central role in guiding the differentiation of stem cells into chondrocytes and facilitating the expression of type II collagen (Col II) [18]. Empirical evidence posits that TGF-β1, upon binding to its cognate ligand, instigates the activation of the TGF-β/Smad pathway, thereby fostering the differentiation of stem cells and the expression of crucial chondrocyte markers, including Sox-9 and Col II [19]. Moreover, the PI3K/AKT pathway has emerged as a participant in the regulatory processes governing Col II expression in chondrocytes [20]. It is theorized that eukaryotic translation initiation factor 4E-binding protein 1 (4ebp1), positioned as a downstream effector of AKT, plays a substantive role in modulating Smad translation levels. This modulation, in turn, exerts influence over downstream gene expression within the TGF-β/Smad pathway. Consequently, this intricate interplay culminates in the heightened synthesis of Col II and proteoglycans, exemplified by Aggrecan (Agc) [21]. The cumulative result is the induction of a chondrogenic effect within the composite framework of dECM, BMSCs, and EVs derived from BMSCs, encapsulated in the context of dECM-BMSCs-EVs [22].

Through the utilization of pre-defined trajectories, 3D bioprinting emerges as a transformative methodology for crafting personalized tissue repair scaffolds. These scaffolds, composed of a synergistic blend of biological materials, cells, and growth factors, hold significant promise for advanced regenerative applications [23]. In our latest endeavors, we have pioneered the formulation of a novel bioprinting ink specifically tailored for cartilage tissue repair, grounded in the principles of Electro-Writing (EW) [24,25]. Distinguished by its exceptional attributes, our EW-based ink exhibits remarkable biocompatibility and bioactivity, rendering it exceptionally well-suited for the intricacies of cartilage tissue regeneration.

In this investigation, we scrutinized the synergistic influences of EVs and dECM in the context of cartilage injury repair, along with an exploration of the associated pathways. For this purpose, EVs sourced from chondrocyte-derived dECM were employed. Additionally, we utilized advanced EW technology, known for its high precision, to craft a meticulously designed cartilage repair scaffold characterized by elevated porosity. This scaffold demonstrated exceptional biocompatibility and bioactivity. Subsequent to the fabrication, a comprehensive series of in vitro and in vivo experiments was executed to authenticate the biological activity and efficacy of the scaffold in cartilage repair.

2. Materials and methods

2.1. Preparation and verification of materials

2.1.1. Preparation of dECM

Fresh pig meniscus was processed by chopping, freezing, and grinding into a powder. The powder was treated with pancreatin, ethanol, hydrogen peroxide, Triton-X, EDTA, and Tris, followed by washing with water and centrifugation. The resulting precipitate, rich in extracellular matrix, was stored at −80 °C. After freeze-drying to preserve its structure, the precipitate was ready for further use.

To prepare the dECM, it was combined with HCl and pepsin, stirred for 2 h at 21 °C, and adjusted to pH 7 with NaOH. After freezing and lyophilization, the powder was washed with water and lyophilized again.

2.1.2. Cell extraction and cultivation

All procedures involving animals and experiments in this study were ethically approved by the Animal Ethics Committee of the First Affiliated Hospital of Zhengzhou University (2019-KY-108). 2-4-week-old Sprague-Dawley (SD) rats were used to isolate bone marrow mesenchymal stem cells (BMSCs). Femurs and tibias were dissected, cleaned, and washed with α-DMEM medium containing high glucose, fetal bovine serum, penicillin-streptomycin, and heparin sodium. Wash fluid with cells underwent centrifugation at 100*g* for 5 min, then isolated cells were suspended in culture medium and seeded. Cultivation occurred in a 5 % CO2 incubator at 37 °C, with medium changes every 2–3 days. This initial cell population was labeled as Passage 0 (P0).

2.1.3. Preparation the EVs

In in vitro experiments, dECM-BMSCs-EVs are extracted from femurs of P3 passage cells using ultracentrifugation. Cells are divided into two groups: one pre-treated with meniscus dECM (dECM-BMSCs group) and the other serving as a normal BMSCs control group. After reaching 80 % growth, cells are cultured in serum-free medium for 48 h before harvesting the medium. The collected medium undergoes centrifugation at 500×*g* for 5 min and 2000×*g* for 20 min. Supernatant is discarded, and cellular components are removed. The supernatant is then ultracentrifuged at 100,000×*g* for 1 h, filtered, and centrifuged again at 100,000×*g* for 3 h. Isolated EVs (dECM-BMSCs EVs) are obtained by resuspending and precipitating them in a 100 μl PBS solution, ensuring purified extracellular vesicles for further analysis.

The identification of EVs involved a multifaceted approach utilizing advanced techniques. The morphological characterization was undertaken using Transmission Electron Microscopy (TEM), enabling a detailed observation of the EVs at the nanoscale level. Nanoparticle Tracking Analysis (NTA) was employed for the precise measurement of EV size, providing valuable insights into their dimensional characteristics. To ascertain the properties of these EVs, the surface marker protein was investigated, allowing for a comprehensive understanding of their

molecular composition and functional attributes.

Following the extraction of RNA, an appropriate volume was diluted using the corresponding dilution solution via NR1 cartridges, and subsequent machine detection procedures were implemented. The normalization and analysis of differential expression levels were performed using the DESeq2 package in the R programming environment. Additionally, the Miranda software was utilized to systematically identify differential miRNA targets. In the final stage of analysis, both predicted and experimentally validated target genes underwent comprehensive scrutiny for functional enrichment, encompassing Gene Ontology and Kyoto Encyclopedia of Genes and Genomes (KEGG) enrichment analyses.

2.1.4. Preparation of bioink

The bioink formulation involves a meticulous combination of components. Specifically, 10 mL of sterile double-distilled water is blended with 2.0 g of PEGDA, 10 μg of benzoin phosphinic acid (serving as the photoinitiator), 0.5 g of PEO, and 0.2 g of dECM powder. This precise mixture forms the base for the bioink used in the subsequent extrusion-based 3D bioprinting process. BMSCs should be incorporated at a concentration of 1 × 10ˆ6 cells mLˆ −1. Additionally, to augment the bioink's regenerative potential, EVs are included at a concentration of approximately 1 μg/ml. This comprehensive bioink composition is designed to facilitate the 3D bioprinting process while ensuring a conducive environment for cellular activity and regenerative processes.

2.1.5. Preparation of scaffold

The ambient environment undergoes sterilization through ultraviolet light exposure, concurrently maintaining a regulated temperature of 21 °C. The printing substrate establishes a connection to a negative potential, while the needle assumes a grounded configuration. Precise adjustments are made to the air pressure, set at 0.1 MPa, and the needle-to-printing surface distance, fixed at 3 mm, is accompanied by a voltage of 3 kV. The bio-ink, encompassing BMSCs at a concentration of 1 × 10ˆ5 cells per mL, is meticulously loaded into a pristine printing material syringe connected with a 24g needle. After printing 10 layers, expose the hydrogel to ultraviolet light for 6 s to facilitate cross-linking. For in vivo experimentation, an approximately 1 mm-thick construct (comprising 50 layers) is precisely printed. Following the printing process, the resultant construct is immersed in a sterile PBS solution.

2.2. In vitro biological evaluation

2.2.1. Cell culture and induction

To explore the influence of Bioink on cell adhesion, we initiated experiments by seeding bone marrow mesenchymal stem cells onto the bioink. Subsequently, we conducted a series of assessments encompassing cell migration, biocompatibility, and bioactivity. In our study, both MG63 and BMSCs were utilized to analyze the bioink's capacity for cell spreading and its broader biological effects. Initially, these cells were blended into the bioink for comprehensive investigation.

After the formulation of the Bioink, it was dispensed into a 24-well plate and subjected to a 6-s exposure to UV light for the purpose of solidification. Following this step, the concentration of P2 BMSCs was meticulously set to 30,000 cells/mL, and subsequently, 1 mL of the cell suspension was introduced into each well. To assess cell viability, live and dead cell staining procedures were employed. Furthermore, a comprehensive cell count analysis was executed by observing the samples under a fluorescence microscope.

2.2.2. biocompatibility and proliferation

The biocompatibility of the scaffolds was evaluated through a multifaceted approach. Cell viability was assessed utilizing calcein-AM and propidium iodide (Thermo Fisher Scientific), providing insights into the live and dead cell populations within the scaffold. Furthermore, cell proliferation was gauged through the implementation of the CCK-8 assay (Dojindo, Kumamoto, Japan), a technique that measures cellular metabolic activity and serves as an indicator of cell growth.

2.2.3. Cell migration out of the hydrogel

After conducting a routine digestion and centrifugation process, MG63 cells were incorporated into a hydrogel solution, with the cell concentration meticulously adjusted to 1 × 10ˆ5 cells/mL. Following this, 400 μL of the resultant bioink containing cells was introduced into a Transwell chamber (Corning, 6.5 mm, 5 μm) and subjected to a 6-s UV irradiation for solidification. The UV-treated Transwell chamber, housing the solidified Bioink construct, was then strategically positioned within a 24-well plate, and 1 mL of complete culture medium was added. This entire assembly was subsequently placed within a controlled cell culture incubator maintaining an atmosphere of 5 % CO2 at 37 °C. At specified intervals, specifically 24 and 48 h post-incubation, the Transwell chamber underwent fixation with methanol for a duration of 30 min. Post-fixation, staining was accomplished utilizing a 0.1 % crystal violet staining solution. Notably, the chamber's interior was meticulously swabbed with cotton, enabling optimal visualization of migrated cells at the chamber's base. Subsequent microscopic examination facilitated the observation and documentation of dynamic cellular migration.

2.2.4. Protein expression

RNA extraction from each cell group (n = 5) was executed using the RNA MiniPrep kit. Subsequently, the qScriptTM cDNA synthesis kit coupled with the MiniOpticon real-time PCR detection system facilitated the reverse transcription of RNA into cDNA. The ABI 7300 Fast machine real-time PCR system was then employed to conduct real-time polymerase chain reaction (rt-PCR) for the analysis of expressed genes. The supplementary table (Sup.Table.1) provides details of the primers utilized for the detection of expression levels of specific genes, including Collagen II (Col II), Collagen I (Col I), Lubricin (Lub), Akt, eIF4EBP1 (4ebp), Smad2, Smad6, and Sox-9 (Sox 9).

Upon completion of the cultivation process, the samples underwent fixation with 4 % paraformaldehyde. Subsequent to a brief immersion in 0.1 % Triton-X for 5 min, the samples underwent three wash cycles with PBS, each lasting 5 min. Following this, the samples were immersed in a BSA solution at 21 °C for 1 h, and excess liquid on the sample surface was carefully blotted with absorbent paper. The subsequent step involved an overnight incubation at 4 °C with the appropriate primary antibodies. After thorough washing with PBS, the samples were subjected to a 2-h incubation at 21 °C with the corresponding fluorescent secondary antibodies containing TRITC (Abcam, UK). Subsequently, a 1-h incubation with FITC-labeled phalloidin was conducted, followed by a 30-min incubation with DAPI. The prepared samples were then observed under a confocal microscope. The acquired images were subjected to protein expression analysis using ImageJ, enhancing the precision of the investigation into cellular and molecular features.

The protein concentration of the cell lysates that had been isolated with RIPA buffer (Beyotime, China) was determined using the BCA protein assay kit (Beyotime, China). The Western blot analysis technique, as previously described [58], was applied and the primary antibodies used were anti-collagen I (Bioss, bs-0578R), anti-collagen II (Bioss, bs-11929R), anti-lubrican (Bioss, bs-11175R), anti-SOX9 (Bioss, bs-4177R), anti-4ebp (Bioss, bs-2559R), anti-Smad2 (Bioss, bs-0718R), anti-Smad6 (Bioss, bs-23329R), and anti-AKT (Bioss, bs-0115R).

2.2.5. Physical properties of scaffold

Following a 6-h storage at −80 °C, the samples underwent a 24-h freeze-drying process upon transfer to a freeze dryer. The initial weight (W0) of the samples was meticulously recorded. Subsequently, the samples were immersed in double-distilled water at 37 °C. At designated time intervals, the samples were extracted from the water, excess surface water was gently blotted with absorbent paper, and the resulting weight was measured and recorded as W1. The expansion ratio

was calculated as (W1/W0) × 100 % to ascertain the degree of expansion. This iterative process was conducted in quadruplicate (n = 4) to ensure robustness and reliability in the data.

2.3. In vivo biological evaluation

2.3.1. Preparation of animal models

Under aseptic conditions, an experimental model for the repair of femoral condyle cartilage was established in Sprague Dawley (SD) rats. The in vivo investigation comprised three experimental groups: BC (cartilage injury modeling without filling materials), PE (PEGDA/dECM mixed cell scaffold without exosomes), and PEE (PEGDA/dECM/EVs mixed cell scaffold). Male SD rats, aged 3 months and weighing approximately 200–250g, were housed in a controlled environment with a temperature of 27 °C, a 12:12 h light-dark cycle, and 55–65 % humidity. Anesthesia was induced using a mixture of ketamine (50 mg/kg) and xylazine (50 mg/kg). Subsequently, a 3 mm diameter and 1 mm deep cartilage defect were created in the femoral condyle, and the corresponding repair scaffold was placed based on the designated groups. The incision was then meticulously closed in layers. Specimens were collected at 3, 6, 12, and 24 weeks post-surgery (n = 4).

2.3.2. Tissue staining and immunohistochemical staining

Rabbits were humanely euthanized at 3, 6, 12, and 24 weeks post-operation, and specimens were systematically collected for subsequent analysis. The harvested samples underwent a series of preparatory steps, including decalcification, paraffin embedding, and sectioning. Hematoxylin and Eosin (HE) staining were then employed to visualize tissue cell distribution and assess repair conditions. Additionally, the SaffronO-Fast green staining method was applied to evaluate bone and cartilage repair. Immunohistochemistry staining was subsequently performed to observe tissue protein expression. Primary antibodies, including Anti-Col II, 4ebp, Lubrican (Lub), Smad2, Smad6, Akt, and SOX9, were introduced to the samples and allowed to incubate overnight at 4 °C. Following this, corresponding secondary antibodies were applied and allowed to incubate at room temperature for 2 h. Sequential incubation with SABC, 3,3′-Diaminobenzidine (DAB), and counterstaining with hematoxylin ensued. After mounting the samples with a cover slip, microscopic observation and assessment were conducted.

2.3.3. Quantitative analysis and ELISA detection of total collagen

The mechanical properties and collagen composition of the repaired cartilage in the affected region were assessed for each group at 3 and 24 weeks post-surgery. Subsequent to the mechanical testing, samples were gathered for the analysis of total collagen content using the hydroxyproline method and the determination of type II collagen content utilizing the sandwich ELISA method [26–28]. This dual approach enables a comprehensive evaluation of both the overall collagen composition and the specific content of type II collagen, providing insights into the structural and compositional aspects of the cartilage repair over the designated time points [26–28].

2.4. Data analysis

The statistical analysis of the data was performed using SPSS 25.0 statistical software (SPSS, USA). Quantitative data were expressed as the mean ± standard deviation (SD). The independent sample *t*-test and one-way analysis of variance (ANOVA) were employed for data analysis. A significance level of $^*P < 0.05$ was considered statistically significant.

3. Results

3.1. Material preparation and construction of composite scaffold

3.1.1. Preparation of dECM

The choice of pig meniscus as the source for preparing dECM was grounded in its abundance, accessibility, and favorable biological activity. As illustrated in Fig. 1A, the meniscus was extracted from the pig knee joint. Subsequent to sectioning, fixing, and staining with Hematoxylin and Eosin (HE) as well as 4′,6-diamidino-2-phenylindole (DAPI) stains, the tissue was scrutinized under both light and fluorescence microscopy, as depicted in Fig. 1B. This analysis revealed the well-organized structure of the meniscus and the distinct expression of cell nuclei. The utilization of pig meniscus provides a practical and biologically relevant foundation for generating dECM, enhancing the translational potential of the derived matrix for various applications.

Upon decellularization of the meniscus, staining procedures were implemented to assess the removal of cells and associated components. As depicted in Fig. 1C, the decellularization process was successful, a conclusion further substantiated by statistical analysis of DAPI-stained nuclear images (Fig. 1E). While remnants of some fibers and proteins were still observable, the resultant dECM demonstrated the ability to be converted into a self-assembled nanofiber solution following pepsin digestion and reassembly, as illustrated in Fig. 1D. The effectiveness of the decellularization process is critical for maintaining the structural integrity and bioactivity of the extracellular matrix while eliminating cellular elements.

Biocompatibility assessments were conducted on the dECM hydrogel. Upon cell seeding, no adverse effects were observed, and the cells exhibited excellent adhesion to the substrate. The evaluation of cell viability and adhesion morphology was performed using live/dead staining and fluorescence microscopy, as shown in Fig. 1F and G. After infusing the cells into the dECM hydrogel for solidification and culture, confocal microscopy was employed to observe the live/dead-stained hydrogel, revealing robust cell viability, as illustrated in Fig. 1H and Sup.Fig. 1. This set of experiments demonstrates the compatibility of the dECM hydrogel with cells and suggests its potential as a supportive matrix for cell growth and tissue engineering applications.

The investigation extended to additional Cell Counting Kit-8 (CCK-8) assays performed at distinct time points: 4 h, 3 days, and 7 days. The results, as presented in Fig. 1I, indicate substantial cell proliferation. This observation provides conclusive evidence supporting the excellent biocompatibility of the dECM. The continuous and robust cell proliferation over the specified time intervals highlights the dECM's capacity to function as a favorable adhesive matrix for cells. This finding has significant implications for its potential applications in promoting cell growth and tissue regeneration.

3.1.2. Preparation and verification of EVs

After pre-treating BMSCs with a dECM derived from cartilage, we advanced to the cell culture phase and subsequently extracted EVs. In order to gain insight into the structure and particle size distribution of these EVs, Transmission Electron Microscopy (TEM) was employed. The morphology of the extracellular vesicles was observed and is depicted in Fig. 2A and B. The analysis of EVs can offer valuable information about their size, shape, and structural characteristics.

Western blot analysis was performed on cells treated with dECM and on BMSCs. The results indicated a high expression of EV-specific proteins, including CD63, CD9, and CD81, in the dECM-BMSCs-EVs group, as illustrated in Fig. 2C -D. These proteins are commonly associated with the membrane of EVs, providing further evidence of the successful extraction and enrichment of EVs from the treated cells. Moreover, Dio-labeled EVs were observed to be internalized by BMSCs and distributed around the nucleus after staining the EVs and co-culturing them with BMSCs, as depicted in Fig. 2F. This observation suggests that the extracted EVs from the dECM-treated cells have the ability to be taken up by recipient cells, which is a crucial aspect for their potential role in intercellular communication and therapeutic applications.

To achieve a comprehensive understanding, miRNA sequencing was conducted on extracellular vesicles derived from dECM-BMSCs-EVs with BMSCs-EVs used as a control. The analysis identified the top ten differentially expressed miRNAs, as illustrated in Fig. 2E. To further

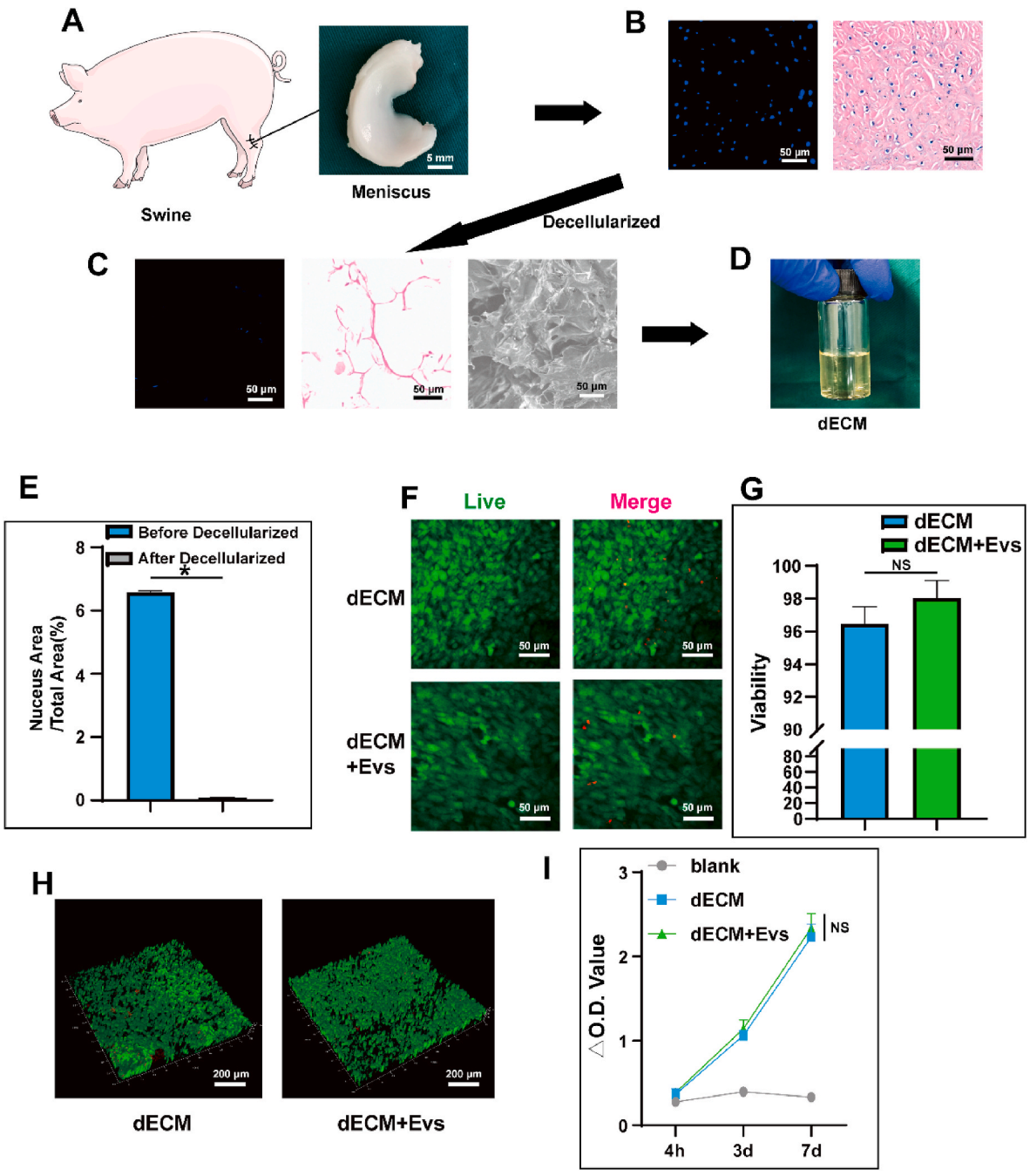

Fig. 1. Preparation, morphology and biocompatibility of dECM. A) Swine and gross view of the meniscus; B) microscopic appearance following HE and DAPI staining of the meniscus; C) SEM images showing microscopic appearance following HE and DAPI staining of the meniscus after being decellularized; D) The dECM after being dissolved; E) Comparison of nucleus area before and after decellularization after DAPI staining; F&G) The live/dead staining performance and viability of BMSCs seeded on dECM hydrogel with/without EVs. H) The live/dead staining performance and viability of BMSCs mixed in dECM hydrogel with/without EVs; I) CCK-8 assay results at various time points of BMSCs seeded on dECM hydrogel with/without EVs. Data represent the mean ± standard deviation (NS > 0.05, *P < 0.05 compared with other groups).

interpret the potential roles and impacts of the identified miRNAs, Gene Ontology (GO) enrichment annotation was applied. The results suggest that dECM-BMSCs-Exos may be involved in the TGF-β/Smad pathway and PI3K/Akt pathway. These pathways are significant in cellular signaling and regulation, and their involvement implies that dECM-BMSCs-EVs could potentially influence cellular processes, including those related to the TGF-β/Smad and PI3K/Akt signaling cascades. Additionally, the findings suggest a potential impact on the protein expression of chondrocytes through the actions of the identified miRNAs, as depicted in Fig. 2G and H.

The identified substantial connections between dECM, EVs, and the Smad and Akt pathways in the context of cartilage repair are noteworthy. Specifically, the inhibition of 4ebp (eukaryotic translation initiation factor 4E-binding protein) emerges as a key factor in these interactions. The inhibition of 4ebp suggests a potential regulatory mechanism in the translation initiation process, which is crucial for protein synthesis.

3.1.3. *Preparation and biological validation of bioink*

Building upon our preceding investigations, we have innovatively

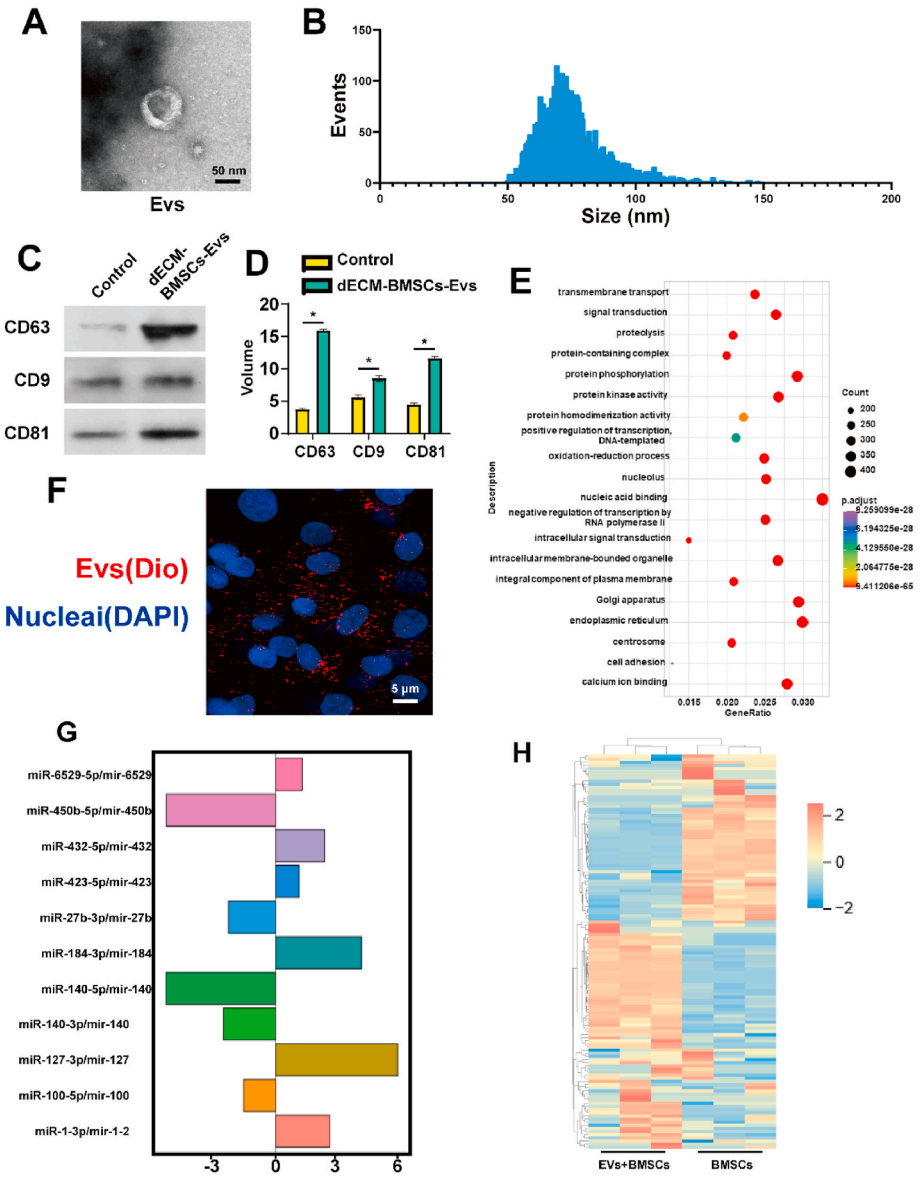

Fig. 2. Preparation, detection and sequencing of EVs. A) SEM images of the EVs; B) Size statistics of EVs; C&D) WB detection and statistics of extracellular vesicle marker protein; E) mRNA sequencing expression difference of dECM-BMSCs-EVs. F) Confocal microscope image of EVs phagocytosis under Dio labeling. G&H) The annotation and possible mechanism of dECM-BMSCS-EVS-related mRNA Gene Ontology (GO) enrichment. Data represent the mean ± standard deviation (*P < 0.05 compared with other groups).

formulated a bioink tailored for Electro-Writing (EW) that is conducive to cell printing and showcases remarkable biocompatibility. Our initial assessments focused on elucidating the cell migration dynamics facilitated by the bioink. Notably, MG63 cells, when integrated with the bioink, exhibited a propensity to migrate out of the hydrogel, subsequently undergoing proliferation over a defined period (Fig. 3A and B; Fig. 3D). Further insights were gleaned through live/dead staining, which underscored the adhesive capabilities of cells within the hydrogel, coupled with their sustained high viability following extended cultivation (Fig. 3C). The application of CCK-8 assays at various temporal intervals—3 hours, 1 day, 3 days, and 7 days—affirmed the robust proliferative potential of the mixed-cell hydrogel. This comprehensive analysis unequivocally corroborates the commendable biocompatibility of our novel bioink (Fig. 3E).

To evaluate the chondrogenic activity of pdECM, EVs, and their combination, Western blotting (WB) and real-time polymerase chain reaction (rt-PCR) analyses were conducted. The results revealed that the combined treatment of dECM and EVs (dECM + EVs) led to an increased expression of chondrogenic markers, including Collagen II (Col II), Collagen I (Col I), Lubrican (Lub), and Akt, compared to individual treatments. Notably, there was a significant decrease in the expression of 4ebp in the dECM + EVs group. The observed downregulation of 4ebp suggests a reduction in the inhibitory effect on protein synthesis, particularly through the Akt pathway. This implies a more effective mitigation of protein synthesis inhibition in the presence of the combined dECM and EVs treatment. Furthermore, the upregulation of Smad2 was noted in both the dECM + EVs and EVs groups, indicating an interaction with the Smad pathway. These findings collectively suggest a coordinated regulatory mechanism. The inhibition of 4ebp, leading to a diminished inhibitory effect on protein synthesis via the Akt pathway, appears to contribute to a more efficient reduction of protein synthesis inhibition. Additionally, the observed interaction with the Smad pathway is indicative of a promotion of chondrocyte-related protein synthesis, exemplified by the increased expression of Col II and Lubrican (Fig. 3F and G). This integrated molecular response highlights the potential synergistic effects of dECM and EVs in enhancing chondrogenic

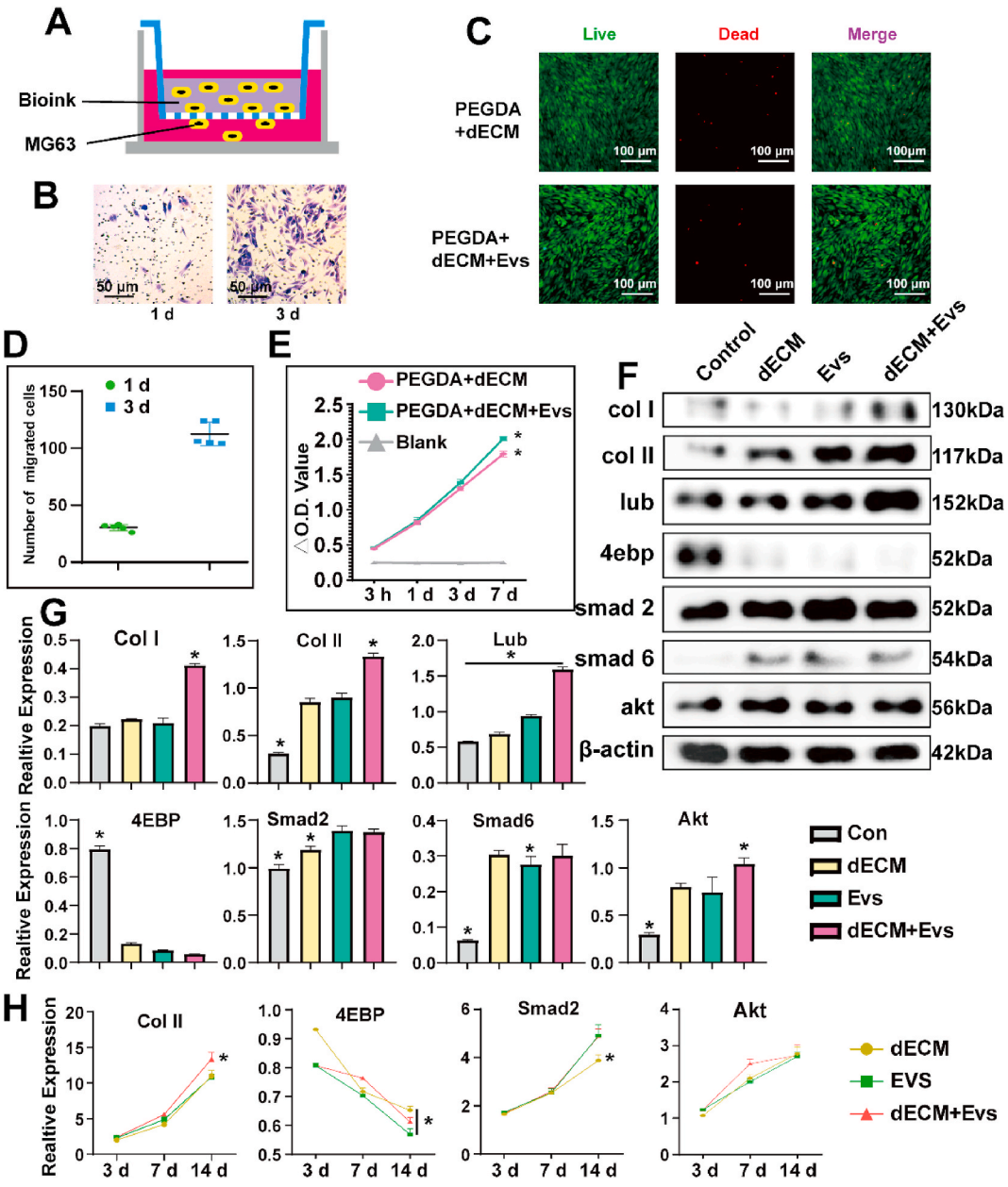

Fig. 3. A&B) Cell invasion experiments with the mixed hydrogel using Transwell. C) The live/dead staining performance of BMSCs seeded on PEGDA/dECM hydrogel with/without EVs. D) Statistical calculation of migrated cells. Data represent the mean ± standard deviation. E) CCK-8 assay results at various time points of BMSCs seeded on PEGDA/dECM hydrogel with/without EVs. F&G) The expression of various proteins in Control, dECM, EVs and dECM + EVs group different groups detected via WB. H) dECM, EVs and dECM + EVs group induce chondrogenesis differentiation and expression of specific proteins shown by rt-PCR. Data represent the mean ± standard deviation (*P < 0.05 compared with other groups).

activity.

The rt-PCR analysis provided additional insights into the expression profiles of key markers in the ECM + EVs group. The results revealed heightened expression levels of Col II, Col I, Lub and Smad2, underscoring the chondrogenic and regulatory activities associated with this combined treatment. Conversely, the expression of 4ebp exhibited a contrasting pattern, aligning with the findings from the Western blotting (WB) analysis (Fig. 3H and Sup.Fig. 2).

Upon conducting meticulous immunostaining and fluorescence microscopy analysis, discernible differences in protein expression were observed upon the combined application of dECM) and EVs. In comparison to the individual impacts of ECM and Evs, cells exhibited an augmented expression of Col II, along with a heightened stimulation of Akt and Smad2. These outcomes suggest a more efficacious promotion of chondrocyte-related proteins under the synergistic influence of dECM and EVs. However, the collaborative effect on the expression of Col I and Sox9 did not reach statistical significance. Specifically, EVs, when administered alone, prompted an increase in the expression of Col I. Intriguingly, when used in tandem with dECM, the expression of Col I exhibited a decrease. Furthermore, the addition of EVs did not yield a notable augmentation in Sox 9 expression (Fig. 4).

These findings underscore the nuanced and context-dependent effects of dECM and Evs interactions on distinct chondrogenic markers. While the combined treatment enhanced the expression of certain markers, such as Col II, Akt, and Smad2, it exhibited a differential impact on the expression of Col I and Sox 9. This intricate interplay highlights the need for a comprehensive understanding of the molecular dynamics involved in dECM and Evs interactions for effective

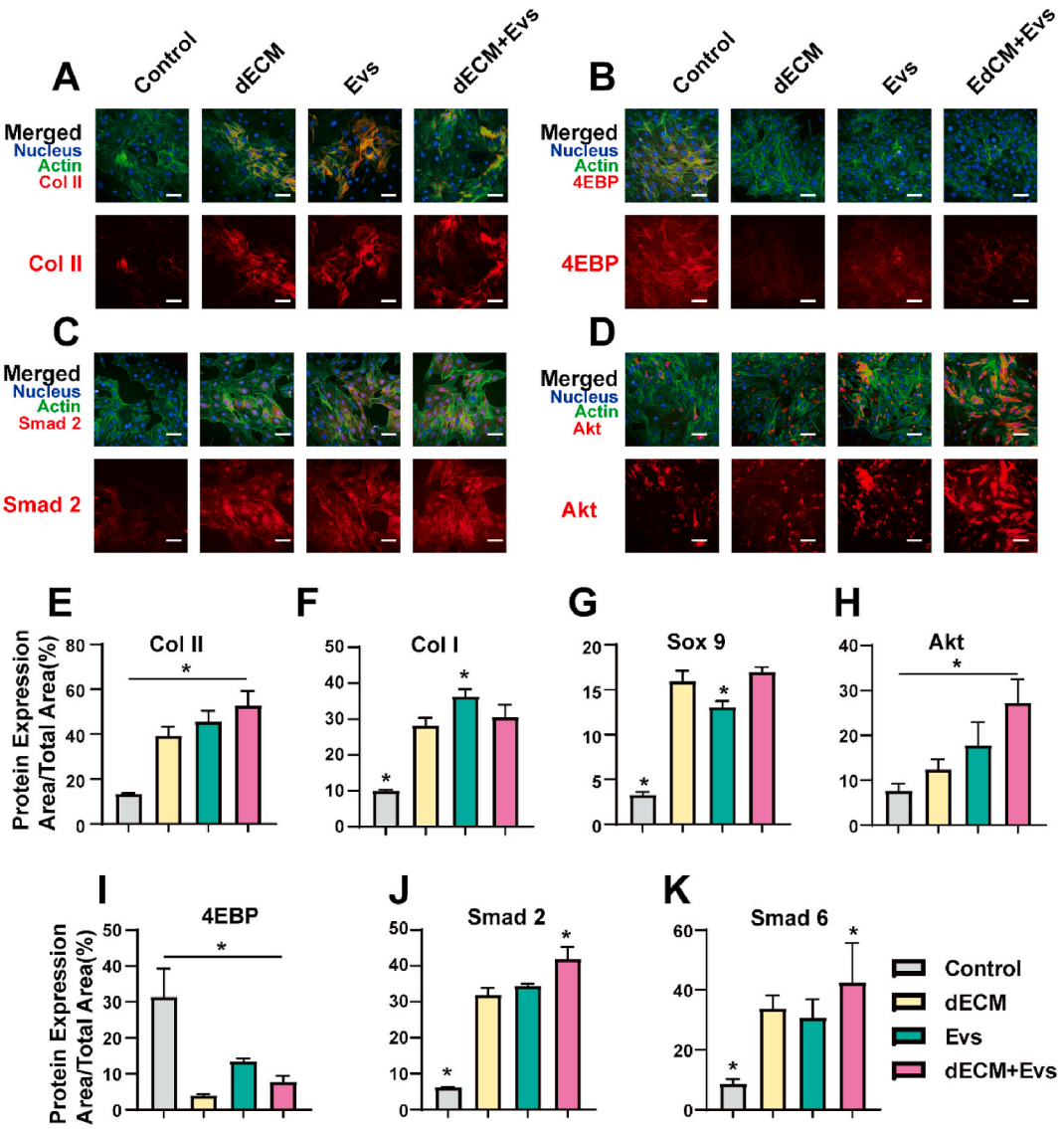

Fig. 4. Control, dECM, EVs and dECM + EVs group induce chondrogenesis differentiation. A-D) Fluorescence microscope images of BMSCs in Control, dECM, EVs and dECM + EVs group detected via immunofluorescence labeling 21 d after cell seeding. Upper panels show "merged" (protein expression + nucleus + F-actin) staining and lower panels show protein expression. E-K) Quantitative evaluation of protein expression via ImageJ software. The results are expressed as protein expression area/total area × 100 (%). Data represent the mean ± standard deviation (Scale Bar: 50 μm) (*P < 0.05 compared with other groups).

modulation of chondrogenic responses.

3.1.4. Fabrication and study of the biologic scaffold

The fabrication process of the scaffold involved the utilization of EW, a technique known for its ability to achieve remarkable printing accuracy, produce thin filament diameters, and generate scaffolds with considerable porosity (Fig. 5A and B). EW is a precise and versatile method for creating three-dimensional structures, particularly in the context of tissue engineering and regenerative medicine. Following the EW process, cross-linking of the scaffold was carried out with the aid of UV light. Subsequently, the scaffold underwent a drying process, and electron microscopy examination (Fig. 5C and Sup.Fig. 3) revealed densely distributed pores within the structure. The retention of the printed structure's solidity indicates successful fabrication and maintenance of the scaffold's architectural integrity.

Our examination of the scaffold's response to swelling, degradation, and protein release elucidated its robust stability during prolonged in vivo exposure. Notably, it exhibited a controlled and deliberate release of internal components (Fig. 5F–H), thereby effecting a precise modification of the local microenvironment to promote and support the repair of cartilage injuries.

To assess the biocompatibility of the scaffold, cell-loaded scaffolds underwent a culture period, with subsequent evaluation through live/dead staining and CCK-8 assays at intervals of 3, 7, and 14 days. The results of these assessments consistently revealed elevated cell viability levels, underscoring the scaffold's exceptional biocompatibility. This observed high cell viability is indicative of the scaffold's capacity to offer robust adhesive support for cells participating in cartilage repair processes (Fig. 5E–I, J). These findings substantiate the scaffold's suitability for fostering favorable interactions with cells involved in tissue regeneration, emphasizing its potential as a biologically compatible platform in the context of cartilage repair.

3.1.5. Study of chondrogenic activity in the bioactive scaffold

Following a two-week cultivation period, the scaffold underwent immunofluorescence staining and subsequent analysis using confocal microscopy. The examination of the scaffold's three-dimensional structure revealed noteworthy insights: dECM + Evs exhibited a

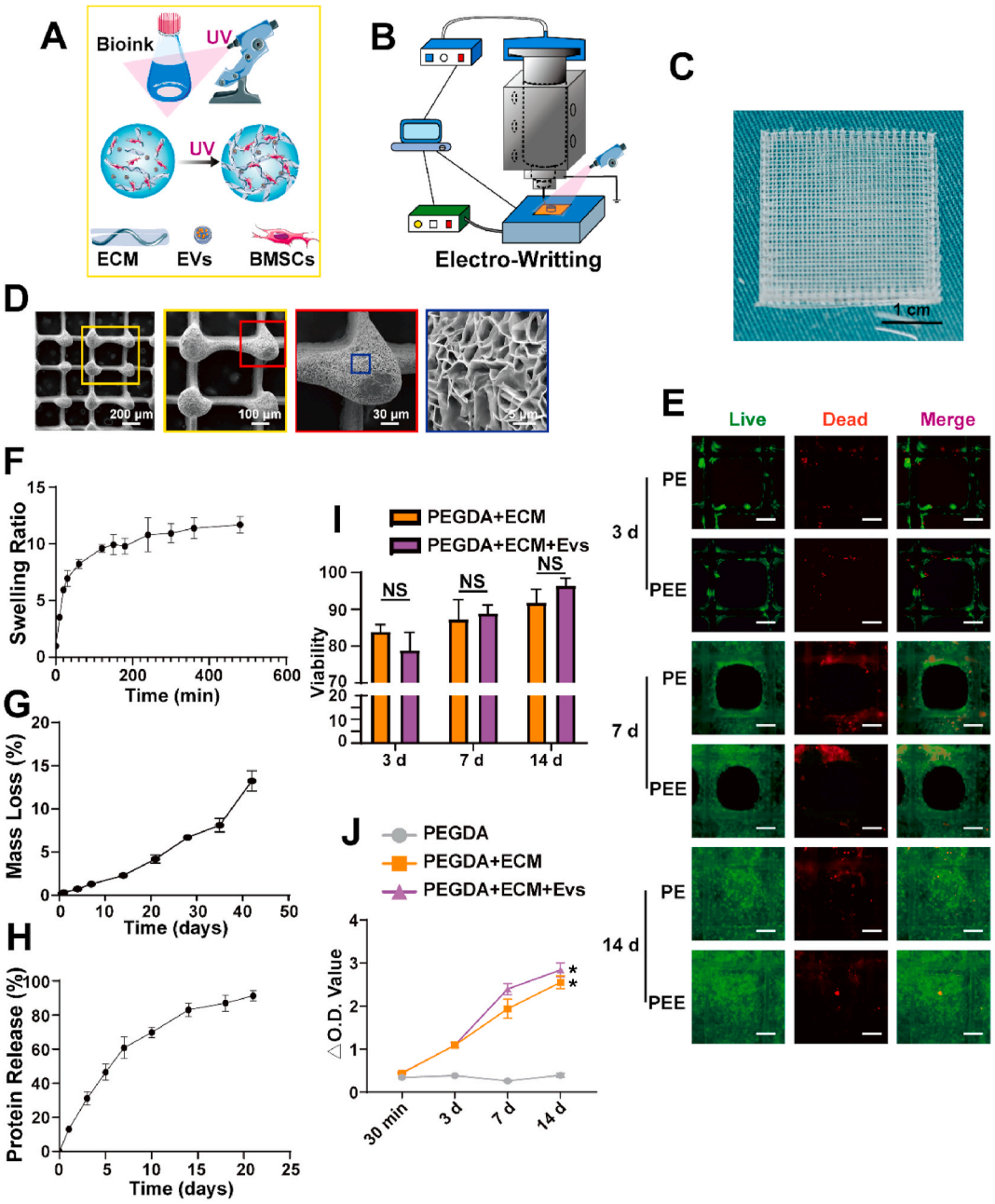

Fig. 5. Preparation and verification of bioactive scaffolds by electro-writing(EW). A) Model diagram of bioink curing; B) Model diagram of EW; C) Gross view of the front face of the scaffold; D) SEM images of thescaffold from the front. E) Live/Dead staining of BMSCs printed, adhered, and proliferated on scaffolds after being printed at 3, 7, and 14 d; F–H) Swelling (F), degradation G), and protein release (H) curves of the composite scaffold; I) Viability of BMSCs on scaffolds after being printed at 3, 7, and 14 d; J) CCK-8 assay results at various time points. Data represent the mean ± standard deviation (Scale Bar: 100 μm) (NS > 0.05, *P < 0.05 compared with other groups).

superior capacity to stimulate the expression of key markers such as Col II, Sox9, Akt, and Smad2 compared to conventional co-culture methodologies. However, the absence of an independent Evs scaffold hindered a direct comparison between Evs and dECM (Fig. A–E; Sup.Fig. 4; Sup.Fig. 5).

Subsequent extraction of tissue mRNA enabled rt-PCR analysis, unveiling that PE + EVs (PEE) showcased a distinct advantage in the expression of markers including Col II, Col I, Smad2, Smad6, and AKT (Fig. 6F-L). These findings underscore the potential of PEE in fostering an environment conducive to the upregulation of crucial markers associated with cartilage repair, indicating a promising avenue for enhanced tissue regeneration. However, the lack of a standalone EVs scaffold remains a limitation, preventing a direct comparison between its effects and those of dECM.

This investigative approach not only validated the significance of the 3D-printed scaffold in the chondrogenic induction process but also unveiled the involvement of critical signaling pathways, including 4ebp, Smad2, and AKT. This nuanced insight into the role of specific signaling molecules further contributes to the comprehensive understanding of the biological mechanisms at play in the context of cartilage regeneration.

3.2. *In vivo biological evaluation*

3.2.1. *Animal model construction*

To strengthen the validity of our findings, we implemented a rat

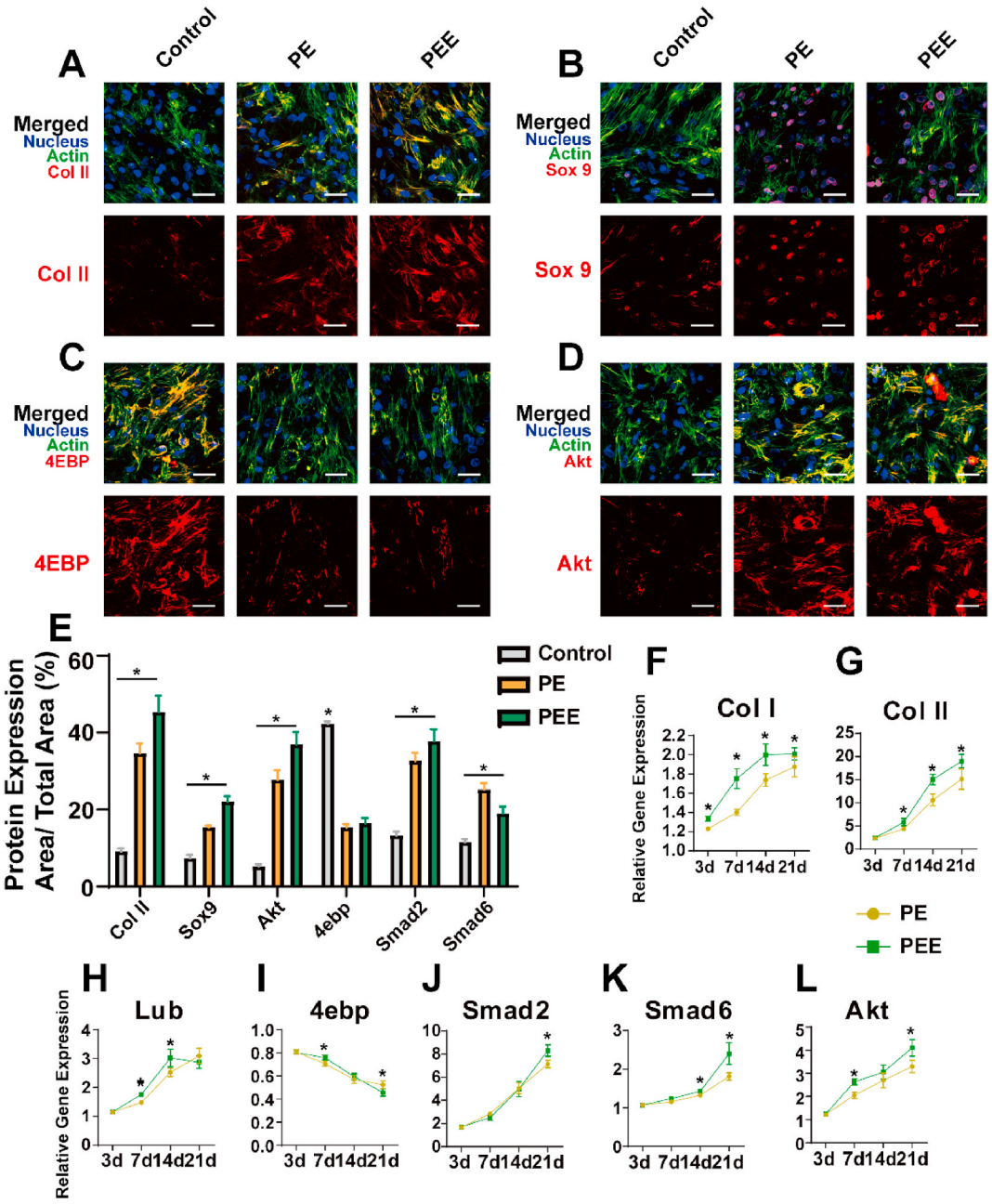

Fig. 6. Control, PEGDA + dECM (PE) and PEGDA + dECM + EVs (PE + EVs) groups scaffolds induce chondrogenesis differentiation. A-D) Confocal images of BMSCs in Control, PEGDA + dECM (PE) and PEGDA + dECM + EVs (PE + EVs) groups detected via immunofluorescence labeling 21 d after cell seeding. Upper panels show "merged" (protein expression + nucleus + F-actin) staining and lower panels show protein expression. B) Quantitative evaluation of protein expression via ImageJ software. The results are expressed as protein expression area/total area × 100 (%). F-L) Groups induce chondrogenesis differentiation and expression of specific proteins shown by rt-PCR. Data represent the mean ± standard deviation (Scale Bar: 50 μm) (NS > 0.05, *P < 0.05 compared with other groups).

femoral condyle cartilage injury model. This involved creating a 3 mm diameter defect encompassing both cartilage and subchondral bone in the distal femoral condyle of the rats' right hind limb. Subsequently, repair scaffolds were implanted in three distinct groups: BC group (Blank Control), PE group (PEGDA + dECM group), and PEE group (PEGDA + dECM + EVs group) (Fig. 7A). This in vivo model provides a relevant and physiological context for evaluating the efficacy of the developed scaffolds in a complex biological environment.

The examination of macroscopic and cross-sectional perspectives of cartilage repair (Fig. 7B and C) revealed distinct trends. Over time, the blank control group exhibited heightened scar formation. In contrast, the PEE group displayed notably enhanced and comprehensive cartilage formation compared to both the PE and blank control groups. Particularly noteworthy was its superior integration with nearby normal cartilage tissue.

At the 24-week mark, MicroCT scanning results indicated a more successful filling and repair of the bone-cartilage defect in the PE and PEE groups compared to the BC group (Fig. 7D). This underscores the crucial role of scaffold-mediated cell adhesion in facilitating effective injury repair.

3.2.2. *Study of in vivo cartilage repair effect*

Histological analysis, employing H&E and Safranin O-Fast Green staining, was conducted to scrutinize the cartilage defect region. H&E staining results for the BC group revealed predominant filling of the injury area with scar tissue, indicative of inadequate integration with

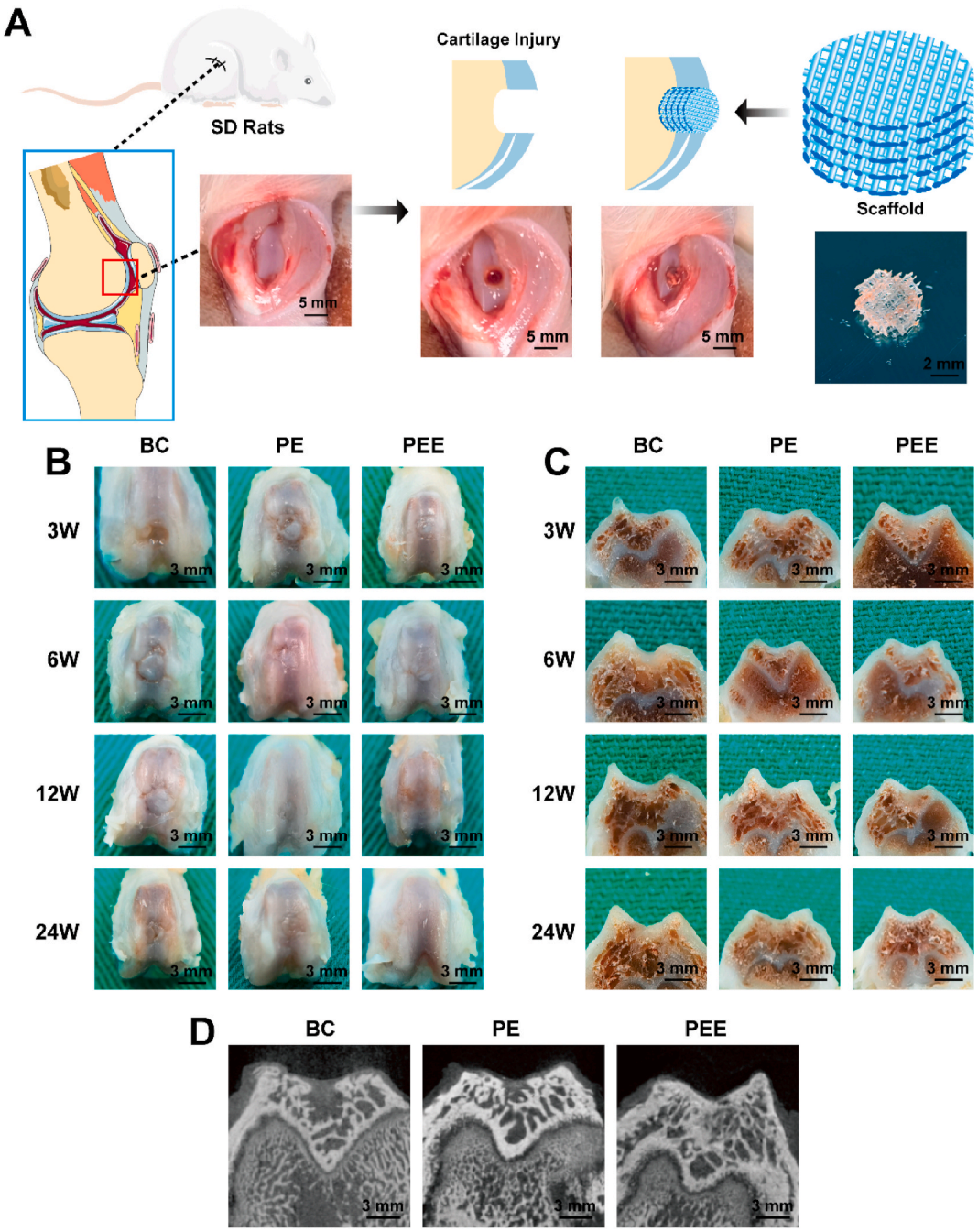

Fig. 7. Schematic diagram of animal experiments. A) Schematic diagram of the SD rats femoral intercondylar cartilage injury model. B) Gross view and C) cross-sectional view of the blank control (BC) group, PEGDA + dECM (PE) group and PEGDA + dECM + EVs (PEE) group 3, 6, 12, and 24 weeks after scaffold implantation. D) Micro-CT images of groups 12 weeks after scaffold implantation.

normal tissue. In contrast, the PE group exhibited a more normative filling of the cartilage injury area, characterized by a substantial amount of cartilage structure, albeit less pronounced than in the PEE group. Notably, at 12 and 24 weeks, the PEE group showcased a normal cartilage cell structure and a well-defined layered cartilage structure, implying a close integration between cartilage and subchondral bone (Fig. 8). This was substantiated by Safranin O-Fast Green staining results (Sup.Fig. 6). Collectively, these findings signify that the PEGDA + dECM + EVs scaffold not only facilitates superior cartilage repair compared to the blank control and PEGDA + dECM groups but also fosters the development of an integrated and well-structured cartilage tissue.

The positive outcomes observed in the in vivo experiments harmonize with the in vitro findings, thus affirming the potential therapeutic efficacy of the developed bioactive scaffold for cartilage regeneration.

Subsequent to immunohistochemical staining of various proteins in the cross-sections, we generated a heatmap visualization for in-depth analysis. Our findings indicate that both the PE and PEE groups exhibited increased expression of Col II, Sox9, Akt, and Smad2. Notably, the combined effect of ECM and EVs was particularly effective in enhancing the expression of Col II. In the BC group, the formation of scar tissue coincided with a significant elevation in Col I expression. The heightened expression of Smad2 and Akt underscored the pivotal role of these pathways in cartilage injury, thus laying a robust foundation for our subsequent investigations (Fig. 9A and B).

Following the implementation of a circular drill to excise the repaired cartilage region, an in-depth examination of its mechanical

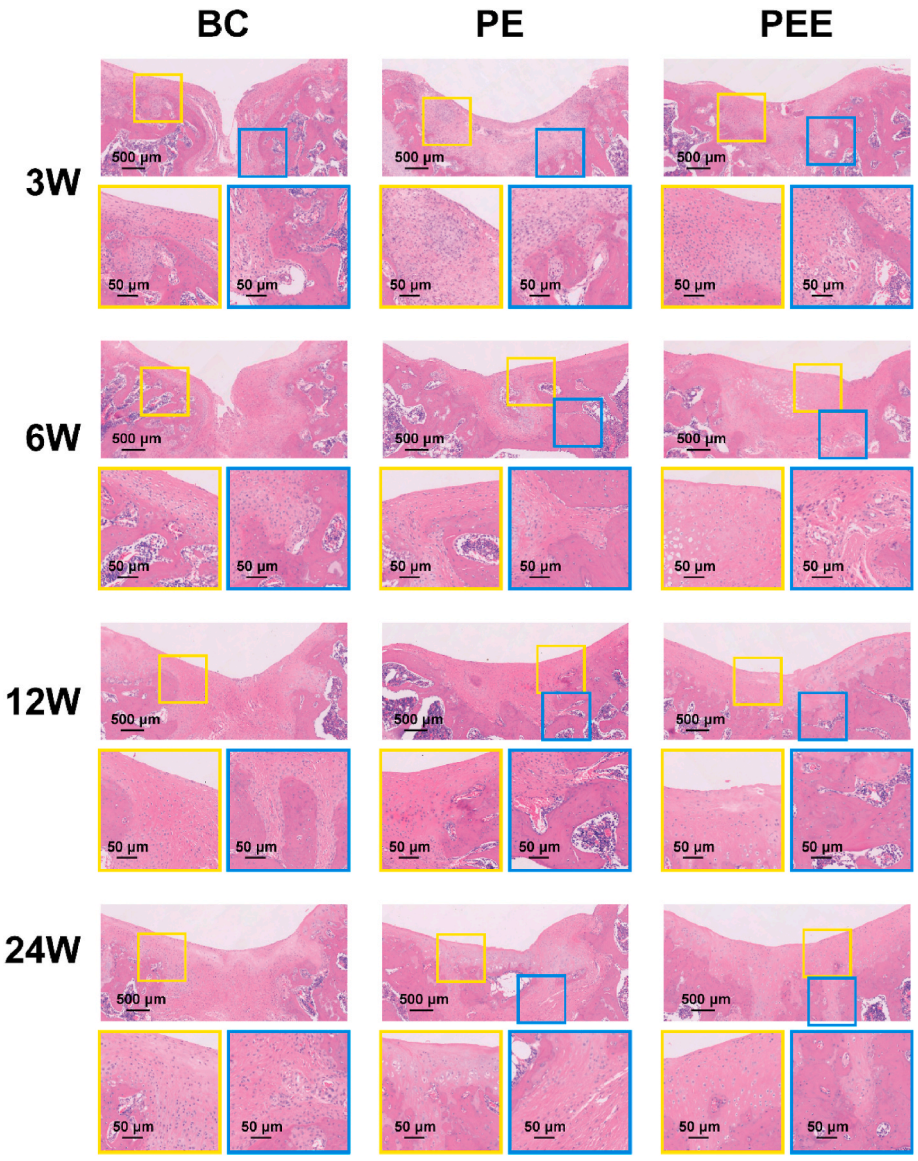

Fig. 8. Microscopic appearance of HE-stained the blank control (BC) group, PEGDA + dECM (PE) group and PEGDA + dECM + EVs (PEE) group after 3, 6, 12, and 24 weeks.

characteristics and collagen composition ensued, as depicted in Fig. 9C–E. Notably, at the 3-week juncture, the BC group predominantly exhibited the presence of scar tissue, concomitant with diminished mechanical properties. In stark contrast, both the PE and PEE groups displayed mechanical attributes incapable of withstanding substantial loads, indicating an ongoing maturation of tissue repair processes.

By the culmination of 24 weeks, a marked elevation in the compressive modulus was discerned across all groups, signifying progressive improvements in mechanical strength. Remarkably, the PEE group stood out with superior compressive strength at this juncture. This temporal evolution underscores the dynamic nature of tissue regeneration, with the PEE group exhibiting advanced mechanical resilience, further corroborating the scaffold's efficacy in fostering not only structural but also functional recuperation of the cartilage.

Our comprehensive analysis affirms and provides insight into the regenerative reparative impact of the PEE group. By systematically collecting and scrutinizing compression samples, we unearthed that the PEE group exhibited a superior capacity for total collagen and Col II production, indicating an enhanced capability for cartilage injury repair. The heightened mechanical properties and optimized collagen composition observed in the PEE group underscore its potential as a promising strategy for successful cartilage regeneration and repair. These findings contribute to a deeper understanding of the therapeutic efficacy of the PEE group in the context of cartilage tissue restoration.

4. Discussion

The investigation of cartilage injury and repair constitutes a pivotal area of emphasis in orthopedic studies [3,29]. Despite this, a comprehensive understanding of the precise mechanisms governing cartilage repair remains elusive. In addressing this knowledge gap, the present research delves into the influence of decellularized matrix and induced extracellular vesicles on the differentiation of stem cells into chondrocytes, probing into potential underlying mechanisms. Furthermore, the utilization of 3D printing technology played a key role in the fabrication of tailored scaffolds designed for in vivo cartilage injury repair, yielding promising outcome. This multidimensional approach underscores the commitment to unraveling the intricacies of cartilage regeneration, blending cellular and biomaterial strategies to advance the field's understanding and therapeutic applications [30–32].

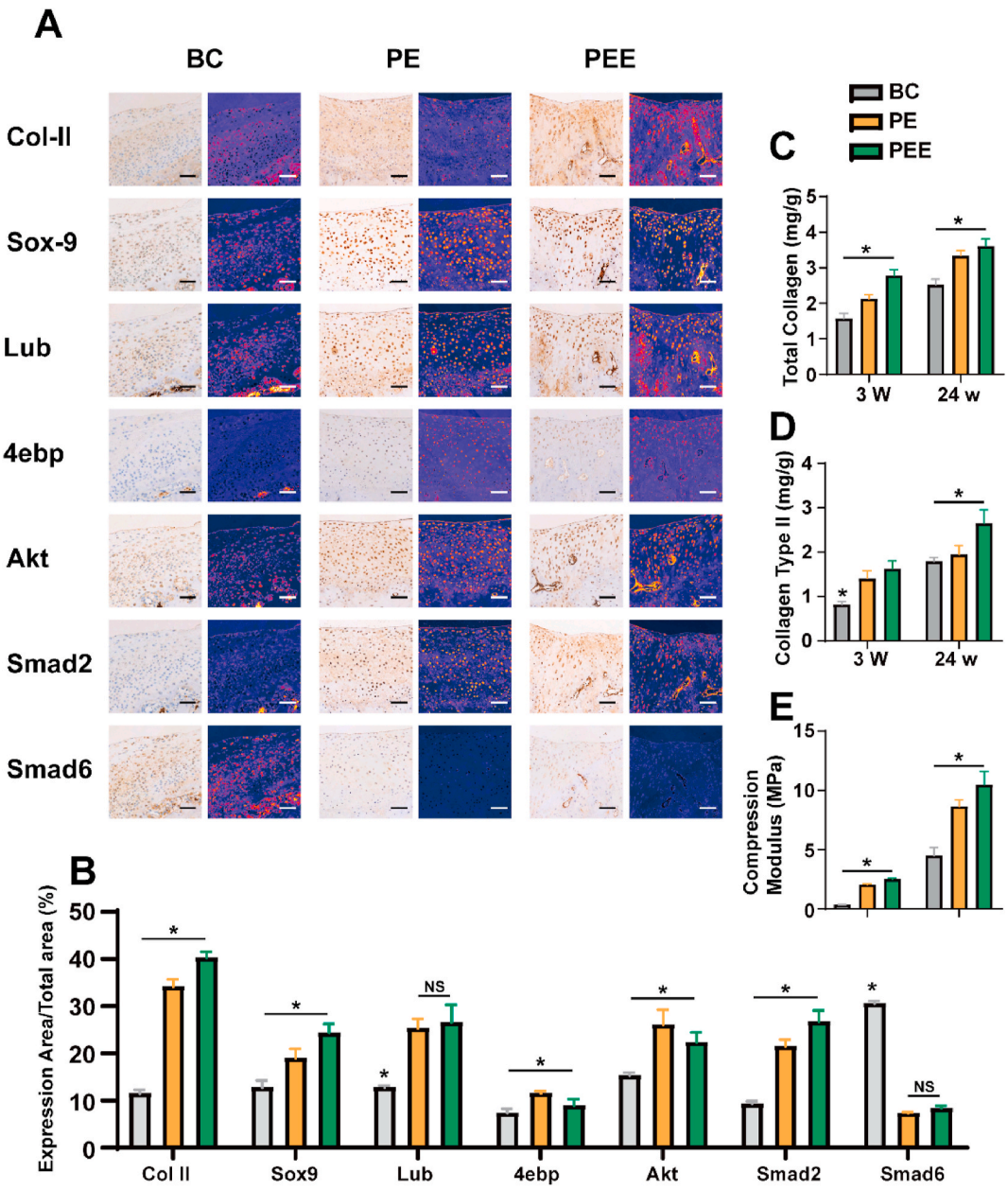

Fig. 9. Composition analysis of regenerated cartilage. A) Immunohistochemical analysis and protein distribution heatmap of various proteins expression levels in the regenerated cartilage of the blank control (BC) group, PEGDA + dECM (PE) group and PEGDA + dECM + EVs (PEE) group after 24 w. B) Analysis of protein distribution. C-E) Composition and mechanical analysis of regenerated cartilage. C) Total collagen content, D) collagen II content, and E) compression modulus of regenerated cartilage in various groups, as indicated, after 3 and 24 w. Data represent the mean ± standard deviation (*P < 0.05 compared with other groups). Data represent the mean ± standard deviation (Scale Bar: 50 μm) (NS > 0.05, *P < 0.05 compared with other groups).

The dECM derived from cartilage exhibits remarkable biocompatibility and bioactivity, demonstrating the capacity to induce the differentiation of stem cells into chondrocytes. The decellularization process, by eliminating immunogenic elements while retaining a substantial quantity of intrinsic cartilage components, effectively preserves the natural microenvironment of cartilage. This preservation of the native microenvironment is crucial for creating an environment conducive to cell differentiation and tissue regeneration. Moreover, the dECM stands out as a suitable choice for cartilage regeneration owing to its abundance and diverse sources [33–36].

While the decellularization process effectively removes immune factors, it is important to acknowledge that as a standalone material, the dECM may inadvertently lose specific bioactive substances, potentially diminishing its overall biological activity. Although the material retains commendable biocompatibility and relatively satisfactory bioactivity, there remains room for further enhancement [37–39].

BMSCs, play a pivotal role in the reparative processes of cartilage tissue. Their significance lies not only in their ability to be recruited in situ but also in their capacity to secrete and regulate the cellular microenvironment, engage in interactions with other cells, and exert therapeutic effects through paracrine pathways. Within this intricate network of signaling, EVs emerge as crucial players, possessing the capability to induce the repair of damaged cartilage. Characterized by a nanoscale size with a double-layer membrane structure and a diameter ranging from 40 to 160 nm, EVs encapsulate biologically active substances, including proteins, nucleic acids, and lipids. This composition equips them to effectively modulate the physiological functions of recipient cells [40].

Emerging research highlights the substantial contribution of EVs to tissue regeneration. Their ability to modulate cellular processes, such as inhibiting apoptosis, promoting cell proliferation, and augmenting extracellular matrix synthesis, positions EVs as promising agents for therapeutic interventions aimed at facilitating tissue regeneration [10,13].

Combining EVs with tissue-specific dECM has proven more efficacious compared to singular applications of EVs or dECM alone in stimulating gene expression during the initial phases of cell differentiation [31]. Moreover, the interaction between EVs and dECM holds promise in enhancing organ function repair. For instance, Zhang et al. demonstrated that co-transplantation of GMSC-EVs and SIS-ECM notably enhanced the restoration of taste bud function [41]. This synergy between EVs and ECM presents a compelling avenue for improving therapeutic outcomes, showcasing their potential in augmenting cellular differentiation processes and facilitating organ function repair.

The microenvironment exerts a profound influence on stem cell behavior, significantly impacting the tissue repair process. This precision in microenvironmental regulation is crucial for steering stem cells along specific differentiation pathways and fostering an environment conducive to effective tissue repair.

In this investigation, sequencing analysis was conducted on induced cartilage cells and stem cells to scrutinize associated pathways. Our observations suggest a notable correlation between the cartilage repair process and the Smad and Akt pathways, wherein 4ebp emerges as a key player. The primary function of 4ebp involves impeding the association between eIF4E (eukaryotic initiation factor 4E) and eIF4G (eukaryotic initiation factor 4G) by binding to eIF4E, thereby obstructing the formation of the translation initiation complex—a critical process in early protein synthesis. Notably, the Akt pathway counteracts this inhibition by phosphorylating 4ebp, relieving its binding to eIF4E and enabling the eIF4E-eIF4G interaction, consequently fostering protein synthesis [21,42].

The Transforming Growth Factor-β (TGF-β) signaling pathway stands as a pivotal contributor to the differentiation of stem cells into chondrocytes and the subsequent formation of type II collagen, with 4ebp emerging as a critical factor in orchestrating this intricate process. By fostering Smad2 activation and concurrently inhibiting Smad6, 4ebp plays a decisive role in augmenting cellular activity, energy utilization, and collagen synthesis. Preliminary research has been undertaken to delineate the pathways and proteins implicated in this phenomenon. However, a more in-depth exploration of the internal mechanisms governing these processes is imperative, prompting the initiation of further investigations [43–46].

This research focuses on leveraging dECM and EVs to formulate an innovative bioink intended for application in Electro-Writing (EW) technology, which holds pivotal significance [47]. Among various 3D printing methodologies, extrusion-based printing stands out as the most prevalent due to its operational ease, cost-effectiveness, and compatibility with a wide spectrum of materials [48]. However, its precision is constrained by the limitations of the printing nozzle, prompting further advancements in accuracy. EW technology, predicated on the manipulation of electrostatic fields, offers a promising solution to enhance precision in printing, achieving accuracies as fine as 1 μm [49,50]. Utilizing this technique can mitigate the precision constraints encountered in conventional extrusion-based printing. Consequently, scaffolds engineered via this method exhibit properties more conducive to cartilage tissue repair [22,51,52].

The investigation involved the formulation of a novel hydrogel bioink by combining PEGDA (polyethylene glycol diacrylate) and dEC, integrating EVs to facilitate its suitability for EW technology. The resultant bioink was noted for its biocompatibility and pronounced bioactivity. Leveraging this precise and porous scaffold, the study effectively addressed cartilage injury, showcasing the scaffold's exceptional biocompatibility and bioactivity in treating such injuries. This outcome underscores the potential efficacy of the developed hydrogel bioink for cartilage repair applications, owing to its favorable properties and bioactivity within the targeted tissue environment.

The scaffold utilizes cartilage tissue's dECM, preserving key elements to enhance chondrogenic differentiation in BMSCs. Loading BMSCs amplifies the repair effect, and its precise, porous structure enables universal and versatile fabrication in tissue engineering.

The study acknowledges certain limitations. Firstly, it conducted preliminary explorations into the molecular mechanisms of dECM andEVs, with a focus on repair effects and relatively superficial mechanistic studies. Further research is crucial for a deeper understanding. Secondly, rats were chosen as the animal model due to antibody source limitations; however, using larger animal models in the future could yield more accurate results. Additionally, the study did not include growth factors, potentially impacting cell induction into cartilage. Despite these limitations, the overall effect is promising. Anticipating more exciting results in subsequent research will further advance the understanding of cartilage injury and repair.

5. Conclusion

The study investigated the synergistic effects of dECM and chondrocyte-derived EVs on repairing cartilage injuries, along with the potential molecular mechanisms involved. The collaboration of dECM and EVs was found to promote cartilage repair through the 4ebp and Smad2 signaling pathways. To further enhance cartilage tissue regeneration and repair, a novel bioink composed of PEGDA and dECM, mixed with EVs, was utilized to create a cell-laden EW scaffold. This scaffold demonstrated high precision, porosity, and biological activity.

Funding

This work was supported by National Natural Science Foundation of China, China (No. 82202685, 82102540, 82100964, 82002283), The First Affiliated Hospital of Zhengzhou University, China (LHGJ20220355).

CRediT authorship contribution statement

Yu Han: Writing – original draft, Methodology, Conceptualization. **Yixin Dong:** Investigation. **Bo Jia:** Validation, Investigation. **Xiangyu Shi:** Writing – original draft, Data curation. **Hongbo Zhao:** Data curation. **Shushan Li:** Validation, Investigation. **Haitao Wang:** Writing – review & editing, Investigation. **Binbin Sun:** Writing – review & editing, Investigation, Formal analysis, Data curation. **Li Yin:** Supervision, Project administration, Conceptualization. **Kerong Dai:** Supervision, Conceptualization.

Declaration of competing interest

This manuscript has not been published or presented elsewhere in part or in entirety and is not under consideration by another journal. We have read and understood your journal's policies, and we believe that neither the manuscript nor the study violates any of these. There are no conflicts of interest to declare.

Data availability

Data will be made available on request.

Acknowledgments

We acknowledge assistance with the access of analytic instruments from Translational Medicine Center at The First Affiliated Hospital of Zhengzhou University.

Appendix A. Supplementary data

Supplementary data to this article can be found online at https://doi.org/10.1016/j.mtbio.2024.101114.

References

[1] M.P. Murphy, L.S. Koepke, M.T. Lopez, et al., Articular cartilage regeneration by activated skeletal stem cells, Nat. Med. 26 (10) (2020) 1583–1592.
[2] H. Zhang, S. Wu, W. Chen, et al., Bone/cartilage targeted hydrogel: strategies and applications, Bioact. Mater. 23 (2023) 156–169.
[3] S. Muthu, J.V. Korpershoek, E.J. Novais, et al., Failure of cartilage regeneration: emerging hypotheses and related therapeutic strategies, Nat. Rev. Rheumatol. 19 (7) (2023) 403–416.
[4] N. Gerwin, C. Scotti, C. Halleux, et al., Angiopoietin-like 3-derivative LNA043 for cartilage regeneration in osteoarthritis: a randomized phase 1 trial, Nat. Med. 28 (12) (2022) 2633–2645.
[5] Z. Peng, H. Sun, V. Bunpetch, et al., The regulation of cartilage extracellular matrix homeostasis in joint cartilage degeneration and regeneration, Biomaterials 268 (2021) 120555.
[6] S. Lee, J. Seo, Y.H. Kim, et al., Enhanced intra-articular therapy for rheumatoid arthritis using click-crosslinked hyaluronic acid hydrogels loaded with toll-like receptor antagonizing peptides, Acta Biomater 172 (2023) 188–205.
[7] M. Brown, J. Li, C. Moraes, et al., Decellularized extracellular matrix: new promising and challenging biomaterials for regenerative medicine, Biomaterials 289 (2022) 121786.
[8] Q. Li, H. Yu, M. Sun, et al., The tissue origin effect of extracellular vesicles on cartilage and bone regeneration, Acta Biomater. 125 (2021) 253–266.
[9] H.P. Bei, P.M. Hung, H.L. Yeung, et al., Bone-a-Petite: engineering exosomes towards bone, osteochondral, and cartilage repair, Small (2021) e2101741.
[10] Y. Zhong, X. Li, F. Wang, et al., Emerging potential of exosomes on adipogenic differentiation of mesenchymal stem cells, Front. Cell Dev. Biol. 9 (2021) 649552.
[11] X. Li, Y. Wang, Z. Cai, et al., Exosomes from human umbilical cord mesenchymal stem cells inhibit ROS production and cell apoptosis in human articular chondrocytes via the miR-100-5p/NOX4 axis, Cell Biol. Int. 45 (10) (2021) 2096–2106.
[12] Z. Zhang, G. Huang, G. Mao, et al., Characterization of exosomal long non-coding RNAs in chondrogenic differentiation of human adipose-derived stem cells, Mol. Cell. Biochem. 476 (3) (2021) 1411–1420.
[13] X. Xu, Y. Liang, X. Li, et al., Exosome-mediated delivery of kartogenin for chondrogenesis of synovial fluid-derived mesenchymal stem cells and cartilage regeneration, Biomaterials 269 (2021) 120539.
[14] S.C. Tao, T. Yuan, Y.L. Zhang, et al., Exosomes derived from miR-140-5p-overexpressing human synovial mesenchymal stem cells enhance cartilage tissue regeneration and prevent osteoarthritis of the knee in a rat model, Theranostics 7 (1) (2017) 180–195.
[15] Y. Ling, W. Zhang, P. Wang, et al., Three-dimensional (3D) hydrogel serves as a platform to identify potential markers of chondrocyte dedifferentiation by combining RNA sequencing, Bioact. Mater. 6 (9) (2021) 2914–2926.
[16] K. Narayanan, S. Kumar, P. Padmanabhan, et al., Lineage-specific exosomes could override extracellular matrix mediated human mesenchymal stem cell differentiation, Biomaterials 182 (2018) 312–322.
[17] V. Waran, V. Narayanan, R. Karuppiah, et al., Utility of multimaterial 3D printers in creating models with pathological entities to enhance the training experience of neurosurgeons, J. Neurosurg. 120 (2) (2014) 489–492.
[18] J. Chen, L. Chen, J. Hua, et al., Long-term dynamic compression enhancement TGF-beta3-induced chondrogenesis in bovine stem cells: a gene expression analysis, BMC Genom Data 22 (1) (2021) 13.
[19] M.K. Murphy, D.J. Huey, J.C. Hu, et al., TGF-beta1, GDF-5, and BMP-2 stimulation induces chondrogenesis in expanded human articular chondrocytes and marrow-derived stromal cells, Stem Cell. 33 (3) (2015) 762–773.
[20] S.L. Hu, K. Wang, Y.F. Shi, et al., Downregulating Akt/NF-kappaB signaling and its antioxidant activity with Loureirin A for alleviating the progression of osteoarthritis: in vitro and vivo studies, Int Immunopharmacol 78 (2020) 105953.
[21] H.S. Hwang, M.H. Lee, H.A. Kim, TGF-beta1-induced expression of collagen type II and ACAN is regulated by 4E-BP1, a repressor of translation, FASEB J 34 (7) (2020) 9531–9546.
[22] D.G. O'shea, T. Hodgkinson, C.M. Curtin, et al., An injectable and 3D printable pro-chondrogenic hyaluronic acid and collagen type II composite hydrogel for the repair of articular cartilage defects, Biofabrication 16 (2023) 015007.
[23] C.J. Gil, C.J. Evans, L. Li, et al., Leveraging 3D bioprinting and photon-counting computed tomography to enable noninvasive quantitative tracking of multifunctional tissue engineered constructs, Adv. Healthcare Mater. 12 (31) (2023) e2302271.
[24] N. Abbasi, S. Ivanovski, K. Gulati, et al., Role of offset and gradient architectures of 3-D melt electrowritten scaffold on differentiation and mineralization of osteoblasts, Biomater. Res. 24 (2020) 2.
[25] P.D. Dalton, T.B.F. Woodfield, V. Mironov, et al., Advances in hybrid fabrication toward hierarchical tissue constructs, Adv. Sci. 7 (11) (2020) 1902953.
[26] G.K. Reddy, C.S. Enwemeka, A simplified method for the analysis of hydroxyproline in biological tissues, Clin. Biochem. 29 (3) (1996) 225–229.
[27] A. He, H. Xia, K. Xiao, et al., Cell yield, chondrogenic potential, and regenerated cartilage type of chondrocytes derived from ear, nasoseptal, and costal cartilage, J Tissue Eng Regen Med 12 (4) (2018) 1123–1132.
[28] A. He, L. Liu, X. Luo, et al., Repair of osteochondral defects with in vitro engineered cartilage based on autologous bone marrow stromal cells in a swine model, Sci. Rep. 7 (2017) 40489.
[29] H. Zhou, L. Yuan, Z. Xu, et al., Mimicking the composition and structure of the osteochondral tissue to fabricate a heterogeneous three-layer scaffold for the repair of osteochondral defects, ACS Appl. Bio Mater. 5 (2) (2022) 734–746.
[30] C. Intini, M. Lemoine, T. Hodgkinson, et al., A highly porous type II collagen containing scaffold for the treatment of cartilage defects enhances MSC chondrogenesis and early cartilaginous matrix deposition, Biomater. Sci. 10 (4) (2022) 970–983.
[31] P. Guan, C. Liu, D. Xie, et al., Exosome-loaded extracellular matrix-mimic hydrogel with anti-inflammatory property Facilitates/promotes growth plate injury repair, Bioact. Mater. 10 (2022) 145–158.
[32] A. Pandey, M. Hoover, M. Singla, et al., TET1 regulates skeletal stem cell (SSC) mediated cartilage regeneration, Arthritis Rheumatol. 76 (2) (2023) 216–230.
[33] M.L. Hall, B.M. Ogle, Cardiac extracellular matrix modification as a therapeutic approach, Adv. Exp. Med. Biol. 1098 (2018) 131–150.
[34] A. Aazmi, D. Zhang, C. Mazzaglia, et al., Biofabrication methods for reconstructing extracellular matrix mimetics, Bioact. Mater. 31 (2024) 475–496.
[35] M. Zhang, F. Yang, D. Han, et al., 3D bioprinting of corneal decellularized extracellular matrix: GelMA composite hydrogel for corneal stroma engineering, International Journal of Bioprinting 9 (5) (2023) 774.
[36] H. Huang, J. Li, C. Wang, et al., Using decellularized magnetic microrobots to deliver functional cells for cartilage regeneration, Small 20 (11) (2023) e2304088.
[37] C. Zhang, C. Jiang, J. Jin, et al., Cartilage fragments combined with BMSCs-Derived exosomes can promote tendon-bone healing after ACL reconstruction, Materials Today Bio 23 (2023) 100819.
[38] S. Li, Z. Kong, B. Ma, et al., Low miR-182-5p expressing extracellular vesicles derived from human bone marrow stromal cells of subjects with steroid-induced osteonecrosis of the femoral head aggravate disease progression, J. Bone Miner. Res. 38 (7) (2023) 976–993.
[39] S. Deng, H. Cao, X. Cui, et al., Optimization of exosome-based cell-free strategies to enhance endogenous cell functions in tissue regeneration, Acta Biomater. 171 (2023) 68–84.
[40] Z. Li, Y. Wang, S. Xiang, et al., Chondrocytes-derived exosomal miR-8485 regulated the Wnt/beta-catenin pathways to promote chondrogenic differentiation of BMSCs, Biochem. Biophys. Res. Commun. 523 (2) (2020) 506–513.
[41] F.X. Zhang, P. Liu, W. Ding, et al., Injectable Mussel-Inspired highly adhesive hydrogel with exosomes for endogenous cell recruitment and cartilage defect regeneration, Biomaterials 278 (2021) 121169.
[42] M. Jiang, R. Liu, L. Liu, et al., Identification of osteogenic progenitor cell-targeted peptides that augment bone formation, Nat. Commun. 11 (1) (2020) 4278.
[43] H. Shen, Y. Wang, Activation of TGF-beta1/Smad3 signaling pathway inhibits the development of ovarian follicle in polycystic ovary syndrome by promoting apoptosis of granulosa cells, J. Cell. Physiol. 234 (7) (2019) 11976–11985.
[44] J. Ying, P. Wang, S. Zhang, et al., Transforming growth factor-beta1 promotes articular cartilage repair through canonical Smad and Hippo pathways in bone mesenchymal stem cells, Life Sci. 192 (2018) 84–90.
[45] Y. Chen, T. Wu, S. Huang, et al., Sustained release SDF-1alpha/TGF-beta1-loaded silk fibroin-porous gelatin scaffold promotes cartilage repair, ACS Appl. Mater. Interfaces 11 (16) (2019) 14608–14618.
[46] T. Sun, S. Yao, M. Liu, et al., Composite scaffolds of mineralized natural extracellular matrix on true bone ceramic induce bone regeneration through smad1/5/8 and ERK1/2 pathways, Tissue Eng Part A 24 (5–6) (2018) 502–515.
[47] K.A. Van Kampen, E. Olaret, I.-C. Stancu, et al., Hypotrochoidal scaffolds for cartilage regeneration, Materials Today Bio23 (2023) 100830.
[48] A. Daghrery, I.J. De Souza Araujo, M. Castilho, et al., Unveiling the potential of melt electrowriting in regenerative dental medicine, Acta Biomater. 156 (2022) 88–109.
[49] G. Constante, I. Apsite, H. Alkhamis, et al., 4D biofabrication using a combination of 3D printing and melt-electrowriting of shape-morphing polymers, ACS Appl. Mater. Interfaces 13 (11) (2021) 12767–12776.
[50] A.R. D'amato, X. Ding, Y. Wang, Using solution electrowriting to control the properties of tubular fibrous conduits, ACS Biomater. Sci. Eng. 7 (2) (2021) 400–407.
[51] H. Wu, F. Xu, Y. Luo, et al., 3D bioprinted endothelial cell-microglia coculture for diabetic retinopathy modeling, Biofabrication 15 (4) (2023).
[52] Y. Sun, Y. Huo, X. Ran, et al., Instant trachea reconstruction using 3D-bioprinted C-shape biomimetic trachea based on tissue-specific matrix hydrogels, Bioact. Mater. 32 (2024) 52–65.